

Photo Copy of manuscript sent to
Tony Tomasa for Microstructures '96
Ceramic

Conf.

Corresponds to 96-1019A.

SAND96-1019C

SAND--96-1019C

CONF-9606237-4

RECEIVED

NOV 26 1996

OSTI

**CHARACTERIZATION OF MICROSTRUCTURE AND CRACK
PROPAGATION IN ALUMINA USING ORIENTATION IMAGING
MICROSCOPY (OIM)**

S. Jill Glass,¹ Joseph R. Michael,¹ Michael J. Readey,² Stuart I. Wright,³ and
David P. Field³

¹Sandia National Labs, Albuquerque, NM 87185

²Caterpillar Inc., Peoria, IL 61656-1875

³TSL Inc., Provo, Utah 84604

ABSTRACT

Structure-property relationships form the basis for understanding and predicting materials behavior. Conventional studies of polycrystalline materials have usually focused either on descriptions of the morphological aspects of the microstructure, such as grain size and shape, or on the chemistry and structure of individual boundaries using transmission electron microscopy (TEM). TEM, while capable of determining the misorientation of adjacent grains, can practicably provide information only for a small number of grain boundaries. Clearly a more complete description of the structure of a polycrystal requires the lattice orientations of a statistically significant number of grains, coupled with morphological aspects of the microstructure, such as grain size and shape. This description can be obtained using a relatively new technique known as orientation imaging microscopy (OIM), which utilizes crystallographic orientation data obtained from Backscattered Electron Kikuchi patterns (BEKP), which are collected using a scanning electron microscope. This paper describes the general OIM results for 99.7 and 99.99% Al_2O_3 samples with grain sizes ranging from 4 to 27 μm . The results include image quality maps, grain boundary maps, pole figures, and lattice misorientations depicted on MacKenzie plots and in Rodrigues space. Results were good in that high quality BEKPs were obtained from all specimens. The images

DISTRIBUTION OF THIS DOCUMENT IS UNLIMITED

ph

MASTER

and data readily reveal the grain morphology, texture, and grain boundary structure. Subtle differences in texture and grain boundary structure, as defined by crystallite lattice misorientations, are observed for the different alumina specimens. Distributions of misorientations for cracked boundaries in alumina are compared to the bulk distribution of boundaries and generally larger misorientations are observed.

INTRODUCTION

The behavior of a polycrystal depends upon the properties of the individual grains, their spatial orientation, and the properties and orientations of the grain boundaries. While relationships between grain size and shape and material properties have been studied extensively, the effects of lattice orientations (microtexture) and misorientations between grains (mesotexture or grain boundary texture) have been almost completely ignored because a measurement technique was not available. Many studies have reported that the properties of a polycrystal vary as a function of grain size. For example, in many ceramics a transition from intergranular to transgranular fracture occurs as the grain size increases. Explanations for this include grain boundary impurity segregation and microcracking; however, these may be symptoms of the cause of the transition, rather than the cause itself. The true cause may be that the distributions of lattice orientations and misorientations are changing as the microstructure evolves. Certain boundaries have a higher mobility than others,^{1,2} which may lead to the preferential removal of these boundaries, leaving a microstructure that is less random than it was. If high energy boundaries, which generally correspond to high angle boundaries, are preferentially eliminated this may lead to a microstructure that has more fracture resistant boundaries, with a concomitant increase in the amount of transgranular fracture.³ There is mounting evidence that lattice orientations and boundary types in polycrystals play a crucial role in determining the intrinsic response of the material and its overall properties.⁴ Certain boundaries (special) may dominate the behavior of a material. For example in Ni_3Al , low-angle and $\Sigma 3$ boundaries are strong, whereas all high-angle boundaries are prone to cracking.⁵ Other properties that are different for special boundaries compared to the general population include impurity segregation,⁶ diffusion, mobility, energy, resistivity, and corrosion resistance. The dramatic differences in properties as a function of the misorientations are exemplified by $\Sigma 3$ boundaries on the 110 zone that have energies of 0.01-0.61 J/m^2 , compared to values of $\sim 1 \text{ J/m}^2$ for a totally disordered, general boundary.⁷ The implication is that if one were able to engineer a polycrystal with a high percentage of special boundaries then one would have the opportunity to enhance the material's overall properties.^{8,3}

The misorientation between two grains is completely described by five parameters, three for the lattice misorientation and two for the boundary normal. It is typically the lattice misorientation that is related to the properties of the grain boundaries, although it is clear that the boundary inclination is also important, especially for the special boundaries.⁹ A convenient framework for describing the crystallography of the grain boundary is the coincidence site lattice (CSL) model. The Σ used in the CSL description is the reciprocal

DISCLAIMER

**Portions of this document may be illegible
in electronic image products. Images are
produced from the best available original
document.**

DISCLAIMER

This report was prepared as an account of work sponsored by an agency of the United States Government. Neither the United States Government nor any agency thereof, nor any of their employees, makes any warranty, express or implied, or assumes any legal liability or responsibility for the accuracy, completeness, or usefulness of any information, apparatus, product, or process disclosed, or represents that its use would not infringe privately owned rights. Reference herein to any specific commercial product, process, or service by trade name, trademark, manufacturer, or otherwise does not necessarily constitute or imply its endorsement, recommendation, or favoring by the United States Government or any agency thereof. The views and opinions of authors expressed herein do not necessarily state or reflect those of the United States Government or any agency thereof.

density of coinciding sites. Thus low Σ values indicate low angle boundaries with a high number of coincident sites. It is generally the low- Σ CSLs, boundaries with $\Sigma \leq 29$, that exhibit special properties.⁹ Watanabe proposed that coincident site lattice (CSL) relationships dominate grain boundary and overall behavior. All boundaries are either categorized as low angle boundaries (misorientation angle $< 15^\circ$), high-angle coincidence boundaries having $3 < \Sigma < 29$, and as random high angle boundaries.

Although there is very little information regarding microtexture¹⁰ and mesotexture,^{11,4} and how they are influenced by processing and microstructural evolution, it is well known that preferred orientation or macrotexture (non random distributions of lattice orientations with respect to the specimen axes) can influence the behavior and response of a polycrystal. Macrotexture is one of the prime sources of anisotropy in polycrystalline materials. In structural materials the anisotropy can be in the elastic properties, fracture toughness, and strength. Macrotexture measurements indicate that directionally-dependent processing techniques, such as hot-pressing and forging, lead to preferred orientations. During hot-pressing, which is the approach used to densify many ceramics, both grain rotation, and preferred grain growth can contribute to the development of macrotexture.¹² Strong basal textures are produced in hot-pressed or forged alumina.¹³

Macrotexture measurements are usually made using X-Ray or neutron diffraction techniques. The results are expressed by pole figures and random orientations produce pole densities of one. Values greater than or less than one indicate that the material has macrotexture. Several pole figures of independent hkl are used as the input data for calculations of the orientation distribution function (ODF). The ODF provides information on the volume fraction of crystals with a given orientation.

Although the results of X-Ray and neutron diffraction macrotexture measurements suggest the presence of a higher than random distribution of special boundaries in many materials, these characterization techniques are unable to provide specific information on the orientation relationship between individual grains (mesotexture or grain boundary texture), or on the relationship between the distribution of lattice orientations and microstructural features such as grain size and grain shape (microtexture). For example, are specific orientations associated with the large or small grains in the microstructures? Also small components of macrotexture may be missed, or complementary texture components with similar volume fractions may cancel each other out producing the effect that no texture is detected. Thus models based on ODF macrotexture data may not be detailed enough to provide valid structure-property relationships.

Even in the absence of directionally dependent processing, and when there is no evidence of macrotexture, microtexture and mesotexture may be present because they are the natural outcome of microstructural evolution. As mentioned earlier, a higher than random frequency of special boundaries may be present after grain growth because certain boundaries are likely to be preferentially eliminated. Certain boundaries have a higher velocity because of their higher mobility and/or the higher driving forces for their migration. This is especially true for materials with a plate-like morphology.¹⁴ The importance of the mesotexture has been noted for both the development of anisotropic microstructures and abnormal grain growth.¹⁵

Similar to the ODF, the misorientation distribution function or MDF has been developed to help characterize the statistical distribution of grain boundary misorientations in a polycrystal.

Although the role of macrotexture in determining the overall response and anisotropy of a material is well known, the roles of mesotexture and microtexture are largely unknown. The presence and evolution of these texture components may be an alternate explanation for changes in properties as grain size increases, such as the often-observed transition in fracture mode. Once the role of these texture components is understood, the goal would be to manipulate them, in the same way that macrotexture is manipulated, to control and improve the overall properties of the material.

Techniques for obtaining the lattice orientation data include optical mineralogical techniques, etch pits, back-reflection Laue patterns, electron diffraction in the transmission electron microscope (TEM), electron channeling, X-ray diffraction using a conventional laboratory diffractometer or a synchrotron radiation source, Kossel X-Ray diffraction, and electron backscatter diffraction in the SEM. These techniques are reviewed by Wright.¹⁶ Except for electron backscatter diffraction in the SEM, each technique has limitations that prevent the acquisition of data regarding the effects of lattice orientation and grain misorientation on properties. These limitations include low resolution, unavailability of an appropriate radiation source, sample preparation difficulties, and the inability to study large areas of the specimen.

A fairly recent technique for characterizing lattice orientations makes use of backscattered electron Kikuchi patterns (BEKP or also referred to as electron backscattering patterns (EBSP)). The first observations of these patterns were reported in 1954 and called High-angle Kikuchi patterns by Alam et al.¹⁷ The first use of BEKP in an SEM for lattice orientation determination was in 1973 by Venables and Harland.¹⁸ In order to obtain a BEKP, the incident electron beam is focused and held stationary on a feature of interest on a specimen that is tilted about 70° toward the BEKP detector. Inside the specimen, the electrons are inelastically and elastically scattered; some are scattered at high angles and exit the specimen. Some of these backscattered electrons satisfy the Bragg condition and are diffracted into cones. There are two cones for every diffracting plane of atoms. These cones of electrons are detected using a suitably placed phosphor screen or photographic film. The cones are imaged as conic sections but appear as parallel sets of straight lines due to the large apex angle of the cones. Interpretation of the pairs of lines, known as Kikuchi bands, allows the specific orientation of the crystal to be determined.¹⁹

Pioneering work by Dingley, including the introduction of the use of a low light level video camera and on-line computer analysis to aid in the identification of patterns, revealed the potential power of the technique.²⁰ Substantial progress in the last decade in hardware and software has provided a unique opportunity to interrogate the microstructures of materials. Completely automated systems are now available for determining lattice orientations from backscattered electron Kikuchi patterns (BEKPs). More detailed descriptions of the hardware and software routines can be obtained in recent references.^{21,16} Presently a spatial resolution of 200 nm and a precision of 1° can be obtained routinely.¹⁶

Not only does the BEKP technique allow the determination of orientations in a statistically meaningful manner, it can also be coupled with information about morphological parameters such as grain size and shape. The term that Adams et al. coined for this coupled information is Orientation Imaging Microscopy (OIM).²² In OIM, the crystallographic orientation is obtained from automatic indexing of BEKPs. The computer controls the electron beam in the SEM so that BEKPs and the corresponding lattice orientation can be obtained at many points on the sample on a user defined grid. In addition to the orientation, the computer records the x,y coordinates, a parameter characterizing the image quality (IQ) of the corresponding BEKP, and a confidence index(CI) describing the confidence the computer has that the indexing algorithm has correctly identified the lattice orientation. An image can then be generated by mapping any of these parameters onto a color or gray scale and shading each point on the data measurement grid accordingly. Such images enable the spatial arrangement of orientation to be graphically displayed providing visual cues to the connection between morphological features of the microstructure and lattice orientation.

OIM allows consolidation of conventional views of the microstructure (such as grain size, shape, and spatial distribution) with information about the local lattice orientation. The orientation image micrograph includes data that must otherwise be obtained from optical microscopy, scanning electron microscopy, TEM, and X-Ray diffraction. The use of color graphics provides helpful visualizations of the microstructure, microtexture, and mesotexture, but to fully utilize the range of information from BEKP data requires statistical measures of the microstructure such as the ODF and MDF. In addition, plotting both the distribution functions and discrete orientation and misorientation data using a variety of representations can help identify the salient crystallographic elements of the microstructure. In this study, we have used several representations of the crystallographic data including pole figures recalculated from ODFs, MacKenzie plots, and discrete plots of misorientation in Rodrigues space²³. The MacKenzie plot shows only the distribution of the misorientation angle and does not include any information about the axis of rotation.

Quantitative, statistical information on the orientations of thousands of grains in a polycrystal is expected to reveal previously unavailable and unknown characteristics of materials. This information provides a unique opportunity to gain a better understanding of structure-property relationships in polycrystalline ceramics, and the roles of microtexture and mesotexture. OIM is still in its infancy in terms of an understanding of its powers and capabilities, and the number of materials that remain to be analyzed. Although there are many ways of analyzing and interpreting the microtexture and mesotexture data obtained using OIM, it remains to be seen which crystallographic features are most relevant and what insights will be gained in the study of polycrystalline microstructures. It is quite likely that once we have gained a better understanding of the range of information available and its relevance, that some long-standing questions regarding structure-property relationships may be answered.

The objectives of this study were to determine whether useable BEKPs could be obtained for polycrystalline alumina materials and to use OIM to examine microtexture and mesotexture as a function of purity (99.7 and 99.99%) and grain size. We were also

interested in examining the distribution of boundary misorientations along cracks in alumina and comparing them to the distribution of boundary misorientations in the bulk. Details regarding the fracture behavior of these alumina materials can be found in recent references.^{24,25}

EXPERIMENTAL PROCEDURE

Sample Processing

Two commercially available alumina powders (99.7%ⁱ and >99.99%ⁱⁱ) were uniaxially pressed at 28 MPa into disks 25 mm in diameter and approximately 3 mm thick. Disks were subsequently isostatically pressed at 280 MPa. The isopressed density was ~ 57% of the theoretical density, 3.98 g/cm³. The disks were buried in a bed of identical powder in high purity alumina crucibles and fired at 1600°C for 5 hr at a heating rate of 5°C/min and a cooling rate of 10°C/min. To increase grain size, specimens were subsequently fired at 1720°C for times up to 48 hr. Quantitative stereology on SEM micrographs provided mean grain sizes (d_{avg}) of 5, 10, and 27 μm for the 99.99% Al₂O₃, and 4 and 13 μm for the two 99.7% Al₂O₃ materials. The grain size distributions appear to be self-similar as grain size increases but the distribution is broader for the lower purity material. The mean aspect ratio was ~1.5 for the 99.99% Al₂O₃, representing a grain shape close to equiaxed for all grain sizes, and ~2 for the lower purity alumina, representing a more elongated shape. Densities ranged from 98.6% TD for the fine-grained 99.99% material to 99.2% TD for the coarse grained 99.99% material, and from 98.7 to 98.29% TD for the 99.7% Al₂O₃ materials.

Sample Preparation for OIM

Conventional metallographic polishing techniques, which consisted of grinding flat with a 9 μm fixed diamond wheel at applied load of 150 N, followed by polishing with 9, 6, and 3 μm diamond polishing at 150 N, were used to prepare the samples. The final polish was done using colloidal silica for three minutes at 100 N. Samples were lightly coated with carbon to prevent charging effects. Coating does not noticeably degrade the backscattered electron Kikuchi patterns.²⁶

Pattern Collection and Data Analysis

The BEKP analyses were performed using a Philips XL30 tungsten source SEM at a voltage of 30 KeV. The beam current was approximately 5 nA. The SEM was equipped with a low-light silicon-intensified tube (SIT) camera capable of capturing BEKP images at a light

ⁱ Alcoa A16 SG Alumina.

ⁱⁱ AKP-50, Sumitomo Chemical Company, New York, NY

level of 5×10^{-5} lux. BEKP data were obtained over a regular hexagonal grid on the surface of each specimen. The scan on the coarse grained alumina ($d_{\text{avg}}=27 \mu\text{m}$) covered an area of $400 \times 400 \mu\text{m}^2$ with a step size of $2 \mu\text{m}$. The fine grained alumina ($d_{\text{avg}}=5 \mu\text{m}$) was scanned over an area of $200 \times 200 \mu\text{m}^2$ with a step size of $1 \mu\text{m}$. Alumina was indexed using trigonal crystal symmetry with lattice parameters of $a=b=4.76 \text{ \AA}$, and $c=12.99 \text{ \AA}$. The alumina data sets consisted of approximately 46,000 orientation measurements each. BEKP images were transferred to a Silicon Graphics Indy workstation, where TSL's Orientation Imaging Microscopy™ software performed the necessary processing to create the desired data sets of x-y coordinates, Euler angles, image quality, and confidence index measures.

Results and Discussion

Useable backscattered electron Kikuchi patterns (BEKP) were obtained from all five alumina samples. Figure 1 shows the OIM image produced for the $27 \mu\text{m}$ 99.99% alumina sample together and a conventional scanning electron microscope micrograph of the same area. One grain is highlighted with an arrow to indicate its position in both images. Note that the sample was not deliberately etched, but grains are apparent in the conventional SEM micrograph because of chemical etching that occurred during the colloidal silica polishing step. One of the advantages of OIM is that no etching of the samples is required to delineate the grains. Grain sizes were calculated from the OIM images and compared to the results obtained in a previous study where standard stereological analyses were performed on conventional SEM micrographs.²⁴ The average grain size from the OIM image of the largest grain alumina sample was $28 \mu\text{m}$ compared to $27 \mu\text{m}$ from the conventional SEM measurements.

Figure 2 is an image quality map for the $10 \mu\text{m}$, 99.99% alumina sample with darker pixels representing a lower image quality. The image quality measure is not normalized for orientation and so a distinct difference in this parameter is seen from grain to grain. The image quality map is determined from the confidence index measured for each pattern, which is a function of diffuseness of the BEKP image. The diffuseness of the image is related to both the orientations and to the perfection of the material. Grain boundaries produce low image quality because measurement points near the grain boundaries are generally affected by the superposed diffraction patterns from the two grains separated by the grain boundary, resulting in a transition area of random noise between the true orientation measurements in the grain interiors. A crack, which also produces a low image quality, can be seen running from the middle left towards the upper right of the image. Figure 3 shows the same image with the addition of grain boundaries, which are drawn for misorientations between neighboring measurements of greater than 15° . Some regions of the image appear as if each measurement is a different orientation and give a chicken wire appearance. These are regions of low confidence which are assumed have been indexed improperly. All such data can be disregarded in the analysis or corrected for by using a clean-up routine that uses a voting procedure to determine the most likely orientation for a given diffraction pattern.

A more detailed analysis of the points contained within the box in Fig. 3, which appear to be part of a single grain, indicate that two orientations are obtained consistently. The fact

that the orientations measured within this grain are not the same and that the average confidence index for the grain is low, along with the fact that there are similarly oriented, but scattered measurement points within the grain suggests that the indexing algorithm may have difficulty properly indexing the diffraction pattern associated with this grain and others that display the same chicken wire appearance. This ambiguity in pattern recognition for alumina needs to be investigated in more detail. While the orientations from these grains seem to be random, there is a possibility that certain orientations are more likely to produce diffraction patterns that produce non-unique indexing solutions (resulting in low confidence indexes). This would bias the texture results away from these types of orientations. The data set was processed to ignore data from these types of grain using a clean-up procedure. When a point is surrounded by three points with the same orientation then its orientation is changed to match the orientation of those three points. Then the data is grouped into grains by grouping neighboring points whose orientation does not differ more than 5 degrees. Finally, grains with less than 25 measurement points per grain were neglected. This procedure results in the image shown in Fig. 4. The shades in this image are not related to the grain orientations in any way, but are just chosen to help delineate the grains. The clean-up procedure is not entirely effective in eliminating the unreliable data but it allows the noise associated with points near grain boundaries to be eliminated producing a better structure for generating accurate orientation and misorientation distributions.

Figure 5 shows the 002 (using the 3 index notation for hexagonal symmetry) intensity pole figures for each of the alumina samples. The rolling direction (RD) and transverse direction (TD) represent the two directions in the plane of the sample, which is perpendicular to the original uniaxial pressing direction. Figure 6 shows the misorientation distributions as MacKenzie plots, which show the frequencies of given misorientations. The predicted random misorientations for crystals with n -fold dihedral symmetry (where trigonal is represented by $n=3$) are shown in Fig. 7.²⁷ Misorientation data can also be represented in Rodrigues space, which is particularly useful for the display of mesotexture because special boundaries are easily recognized.¹⁹ Misorientations for the 13 μm , 99.7% alumina sample, which appears to exhibit the greatest degree of mesotexture, are shown in Rodrigues space in Fig. 8. Rodrigues space plots for the other samples are not included because of space considerations, but the results are discussed below.

Comparison of the MacKenzie plots in Fig. 6 shows that all samples appear to have a greater frequency of misorientations at angles between 55 and 60° than are indicated in the predicted random distribution in Fig. 7. As discussed earlier, in the alumina crystal structure (trigonal - di-pyramidal), there exist certain orientations for which the solution of the BEKP is ambiguous. We believe that the 60° peak in the plots is an artifact of this indexing difficulty. Other than this anomaly the data in the MacKenzie plots appear to be close to random. The only distribution that is significantly different than the rest is that for the 13 μm , 99.7% alumina sample which also has the least random texture as seen in its pole figure in Fig. 5.

General Features of the Pole Figure Representations of Microtexture and Rodrigues Space Representations of Mesotexture

5 μm , 99.99% alumina. The texture is quite random as seen by the intensity pole figure for the c-axis. The MacKenzie plot is also fairly random. The misorientations plotted in Rodrigues space are somewhat random, but shifted towards c-axis rotations in the distribution (left-hand vertex of each triangle in the space). There are also a number of low angle boundaries (upper-left hand triangle c-axis position).

10 μm , 99.99% alumina. The texture is somewhat random, but some clusters appear to be forming. The pole figure shows the c-axis has a weak component as well as a few positions rotated 50-60° off the c-axis. The Rodrigues space plot of misorientations indicates the presence of some low angle and c-axis misorientations, but also contains a small cluster at a position of 50° about an a-axis.

27 μm , 99.99% alumina. The texture shown in the pole figure is again quite random, and the Rodrigues space plot is similar to that of the 5 μm , 99.99% alumina.

4 μm , 99.7% alumina. The texture is weak, but has a different character than that of any of the others. The c-axes are aligning about 70° off the specimen surface normal, but only in one general direction. Not much is happening by the transverse direction (TD) but there are some significant features near the rolling direction (RD). There appears to be some in-plane near c-axis texture.

13 μm , 99.7% alumina. The texture in this sample is the strongest of all of the aluminas but there are also fewer grains in the data set. The distribution tends to be off the c-axis by about 40° in a random direction. The misorientations show a peak in the same position as that described for the 10 μm , 99.99% alumina. Additional components exist, each of which lie near the boundary of the fundamental region indicating some special, but not well defined symmetries.

Comparison of the Misorientations for a Crack Compared to the Bulk

Figure 9 shows the OIM image and the points across a crack that were used to determine the distribution of misorientations along a crack in the 10 μm , 99.99% alumina sample. Figure 10 is the MacKenzie plot for these misorientations. Low angle misorientations represent transgranular fracture. Although relatively few data were used to construct the histogram in Fig. 10 it does appear that fracture occurs between grains with misorientations generally higher than those found in the bulk. Larger numbers of misorientations will need to be measured to identify the true distribution and to determine whether special boundaries, such as low angles and twin boundaries, are absent from the distribution. This would provide support for the hypothesis that special boundaries are more fracture resistant. Statistical analyses of misorientation distributions for cracks for materials with a range of grain sizes will also provide information on how the structure of the boundaries is changing as a microstructure evolves.

CONCLUSIONS

Polycrystalline alumina samples were characterized using Orientation Imaging Microscopy (OIM). Generally good BEKP data were obtained and were used to produce pole figures showing microtexture and MacKenzie plots and Rodrigues space representations of mesotexture. Some of the data are unreliable because of the ambiguity in indexing some orientations for the alumina crystal structure. Differences in microtexture and mesotexture as a function of purity and grain size are subtle but measurable. Cracks appear to favor higher angle misorientations than the distribution of misorientations in the bulk. Although good data have been obtained it is still unclear what parameters are most relevant and how the structure is changing as the microstructure evolves. Further measurements will need to be made to provide a more complete picture.

Acknowledgments:

The authors thank Desi Kovar for providing the alumina samples. This work was supported by the U.S. Department of Energy under contract No. DE-AC04-94AL85000 at Sandia National Laboratories.

REFERENCES

1. V. Randle, B. Ralph, and D. Dingley, "The Relationship Between Microtexture and Grain Boundary Parameters," *Acta metall. mater.*, 36 [2] 267-273 (1988).
2. G. S. Grest, D. J. Srolovitz, and M. P. Anderson, "Computer Simulation of Grain Growth - IV. Anisotropic Grain Boundary Energies," *Acta metall. mater.*, 33 [3] 509-520, (1985).
3. T. Watanabe, "Grain Boundary Design and Control for High Temperature Materials," *Mater. Sci. Eng.*, A166, 11-28, (1993).
4. V. Randle, "Grain Assemblage in Polycrystals - Overview No. 115," *Acta metall. mater.*, 42 [6] 1769-1784, (1994).
5. H. Lin and D. P. Pope, "Weak Grain Boundaries in Ni₃Al," *Mater. Sci. Eng.*, A192/193, 394-398 (1995).
6. W. Swiatnicki, S. Lartigue-Korinek, and J. Y. Laval, "Grain Boundary Structure and Intergranular Segregation in Al₂O₃," *Acta metall. mater.*, 43 [2], 795-805, (1995).
7. V. Randle, "An Investigation of Grain-Boundary Plane Crystallography in Polycrystalline Nickel," *J. Mater. Sci.*, 30, 3983-3988 (1995).
8. T. Watanabe, "The Impact of Grain Boundary Character Distribution on Fracture in Polycrystals," *Mater. Sci. Eng.*, A176, 39-49 (1994).
9. A. Garbacz, B. Ralph, and K. J. Kurzydowski, "On the Possible Correlation Between Grain Size Distribution and Distribution of CSL Boundaries in Polycrystals," *Acta metall. mater.*, 43 [4] 1541-1547 (1995).
10. T. T. Wang, B. L. Adams, and P. R. Morris, "Development of Orientation Coherence in Plane-Strain Deformation," *Met. Trans.*, 21A, 2223-2236 (1990).
11. V. Randle, "Origins of Misorientation Texture (Mesotexture)," pp. 745-750 in *Textures and Microstructures*, Vol. 14-18, Edited by H. J. Bunge (1991).
12. F. Lee and K. J. Bowman, "Texture and Anisotropy in Silicon Nitride," *J. Am. Ceram. Soc.*, 75 [7] 1748-55 (1992).
13. Y. Ma and K. J. Bowman, "Texture in Hot-Pressed or Forged Alumina," *J. Am. Ceram. Soc.*, 74 [11] 2941-44 (1991).
14. M. S. Sandlin, C. R. Peterson, and K. J. Bowman, "Texture Measurement on Materials Containing Platelets Using Stereology," *J. Am. Ceram. Soc.*, 77 [8] 2127-31 (1994).
15. J. Rodel and A. M. Glaeser, "Anisotropy of Grain Growth in Alumina," *J. Am. Ceram. Soc.*, 73 [11] 3292-301 (1990).
16. S. I. Wright, "A Review of Automated Orientation Imaging Microscopy," *J. Comput.-Assist. Microsc.*, 5 [3], pp. 207-221 (1993).
17. M. N. Alam, M. Blackman, and D. W. Pashley, "High Angle Kikuchi Patterns," *Proc. Roy. Soc.*, 221A, pp. 224-242, (1954).
18. J. A. Venables and C. J. Harland, "Electron Back-Scattering Patterns - A New Technique for Obtaining Crystallographic Information in the Scanning Electron Microscope," *Phil. Mag.*, L2, 1193-1200 (1973).
19. V. Randle, *Microtexture Determination and its Applications*, The Institute of Materials, London, 1992.
20. D. J. Dingley, "A Comparison of Diffraction Techniques for the SEM," *Scanning Electron Microsc.* IV, 273-286 (1981).
21. K. Kunze, S. I. Wright, B. L. Adams, and D. J. Dingley, "Advances in Automatic EBSP Single Orientation Measurements," *proc. of Symposium on Microscale Textures*, eds. B. L. Adams and H. Weiland, *Textures Microstruct.*, 20, 41-54, (1993).

22. B. L. Adams, S. I. Wright, and K. Kunze, "Orientation Imaging: The Emergence of a New Microscopy," *Metall. Trans. A*, 24A, 819-831, (1993).
23. F. C. Frank, "Orientation Mapping," *Metall. Trans. A*, 19A, 403-408 (1988).
24. D. Kovar and M. J. Readey, "Role of Grain Size in Strength Variability of Alumina," *J. Am. Ceram. Soc.*, 77 [7] 1928-38 (1994).
25. D. Kovar, "The Role of Microstructure on the Mechanical Reliability of Alumina Ceramics," Ph.D. Thesis, Carnegie Mellon University, 1995.
26. J. R. Michael and R. P. Goehner, "Advances in Backscattered-Electron Kikuchi Patterns for Crystallographic Phase Identification", pp. 596-597 in *Proc. 52nd Annual Meeting, Microscopy Society of America*, Edited by G. W. Bailey and A. J. Garratt-Reed, (1994).
27. A. Morawiec and D. Field, "Misorientation Angle Distribution of Randomly Oriented Symmetric Objects," submitted to *J. Appl. Cryst.*, 1996.

- Figure 1. The OIM image for the 27 μm , 99.99% alumina sample together with a conventional scanning electron microscope micrograph of the same region. The arrow highlights the same grain in both images.
- Figure 2. Image quality map for the 10 μm , 99.99% alumina sample with darker pixels representing a lower image quality.
- Figure 3. The OIM image of the 10 μm 99.99% alumina with the addition of grain boundaries, which are drawn for misorientations between neighboring measurements of greater than 15° .
- Figure 4. The OIM image of the 10 μm , 99.99% alumina sample after a clean-up procedure was used to minimize the presence of ambiguous patterns. The shades in this image are used only to help delineate the grains.
- Figure 5. The 002 (using the 3 index notation for trigonal symmetry) intensity pole figures for each of the alumina samples.
- Figure 6. The misorientation distributions as MacKenzie plots for each of the alumina samples.
- Figure 7. The predicted MacKenzie plot of random misorientations for crystals with 3-fold dihedral symmetry (trigonal).
- Figure 8. Misorientations displayed in Rodrigues space for the 13 μm , 99.7% alumina sample, which appears to exhibit the greatest degree of mesotexture.
- Figure 9. The OIM image of the 10 μm , 99.99% alumina sample and the points across the crack that were used to determine the distribution of misorientations along a crack.
- Figure 10. The MacKenzie plot for the misorientations of the crack in Fig. 9. Low angle misorientations represent transgranular fracture. Comparison to the plot in Fig. 6 for the same sample reveals a higher percentage of high angle boundaries.

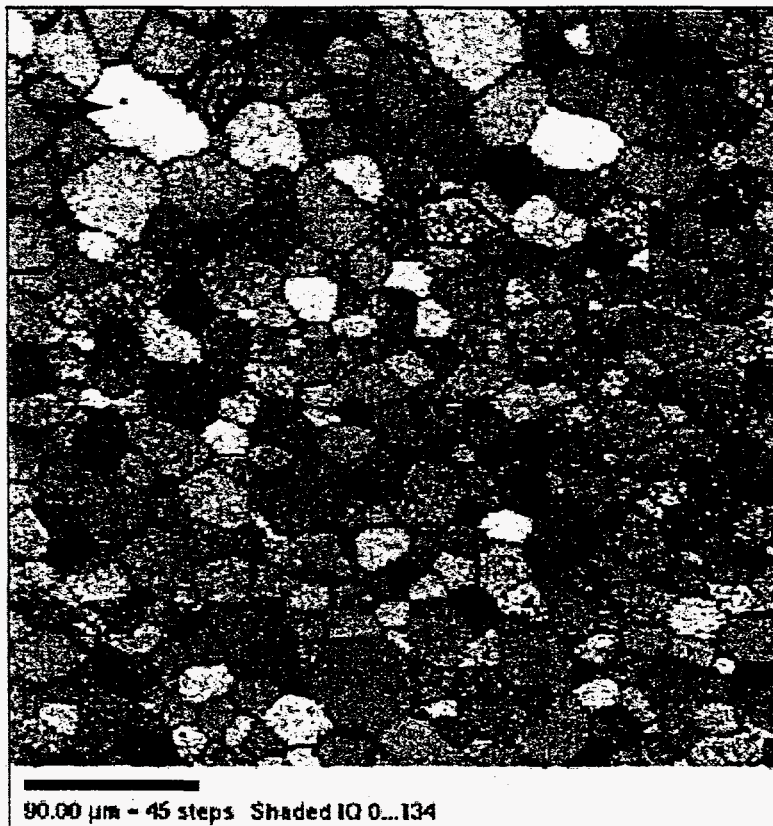
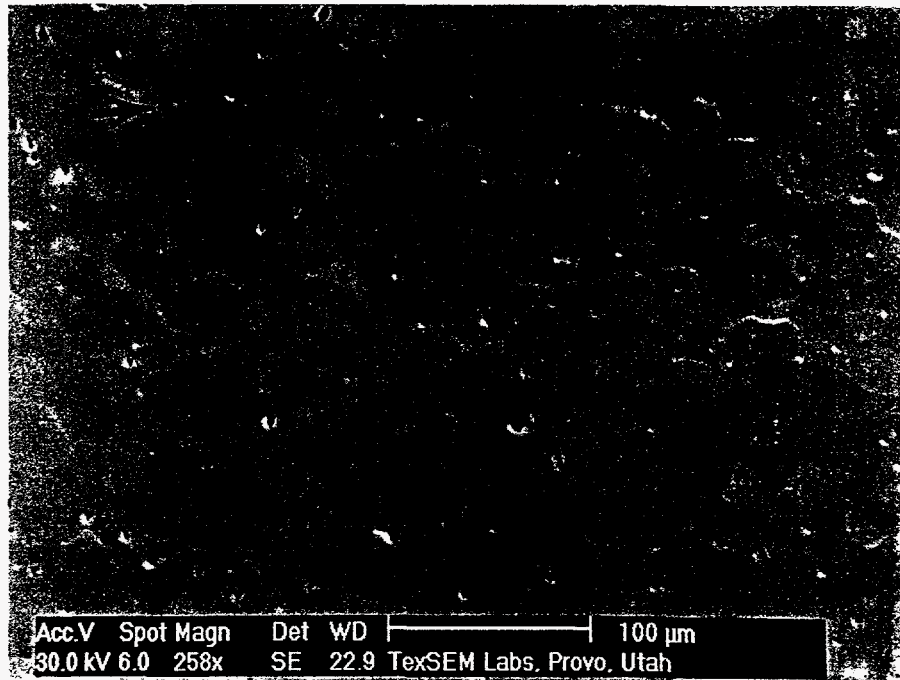


Figure 1. The OIM image for the 27 μm, 99.99% alumina sample together with a conventional scanning electron microscope micrograph of the same region. The arrow highlights the same grain in both images.

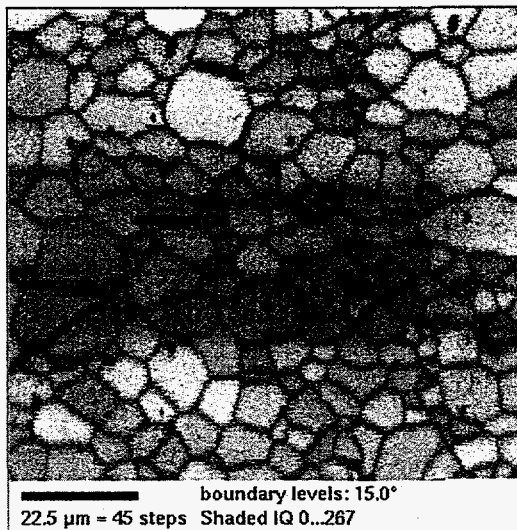


Figure 2. Image quality map for the 10 μm, 99.99% alumina sample with darker pixels representing a lower image quality.

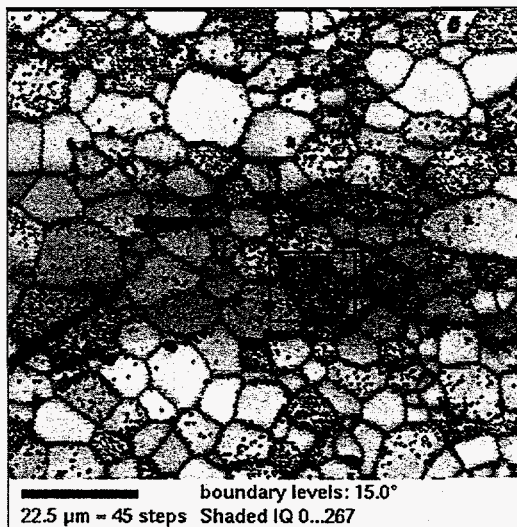


Figure 3. The OIM image of the 10 μm 99.99% alumina with the addition of grain boundaries, which are drawn for misorientations between neighboring measurements of greater than 15°.

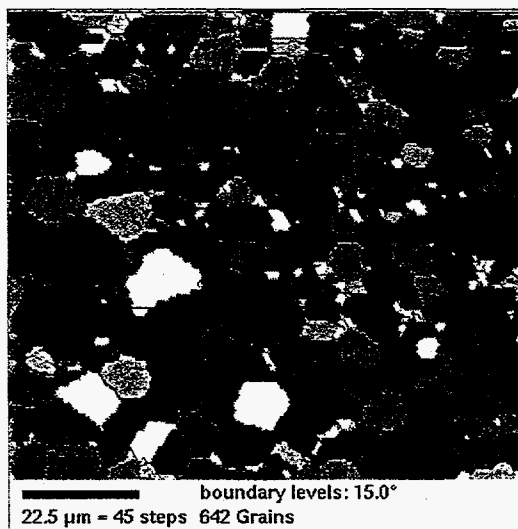


Figure 4.

The OIM image of the 10 μm , 99.99% alumina sample after a clean-up procedure was used to minimize the presence of ambiguous patterns. The shades in this image are only used to help delineate the grains.

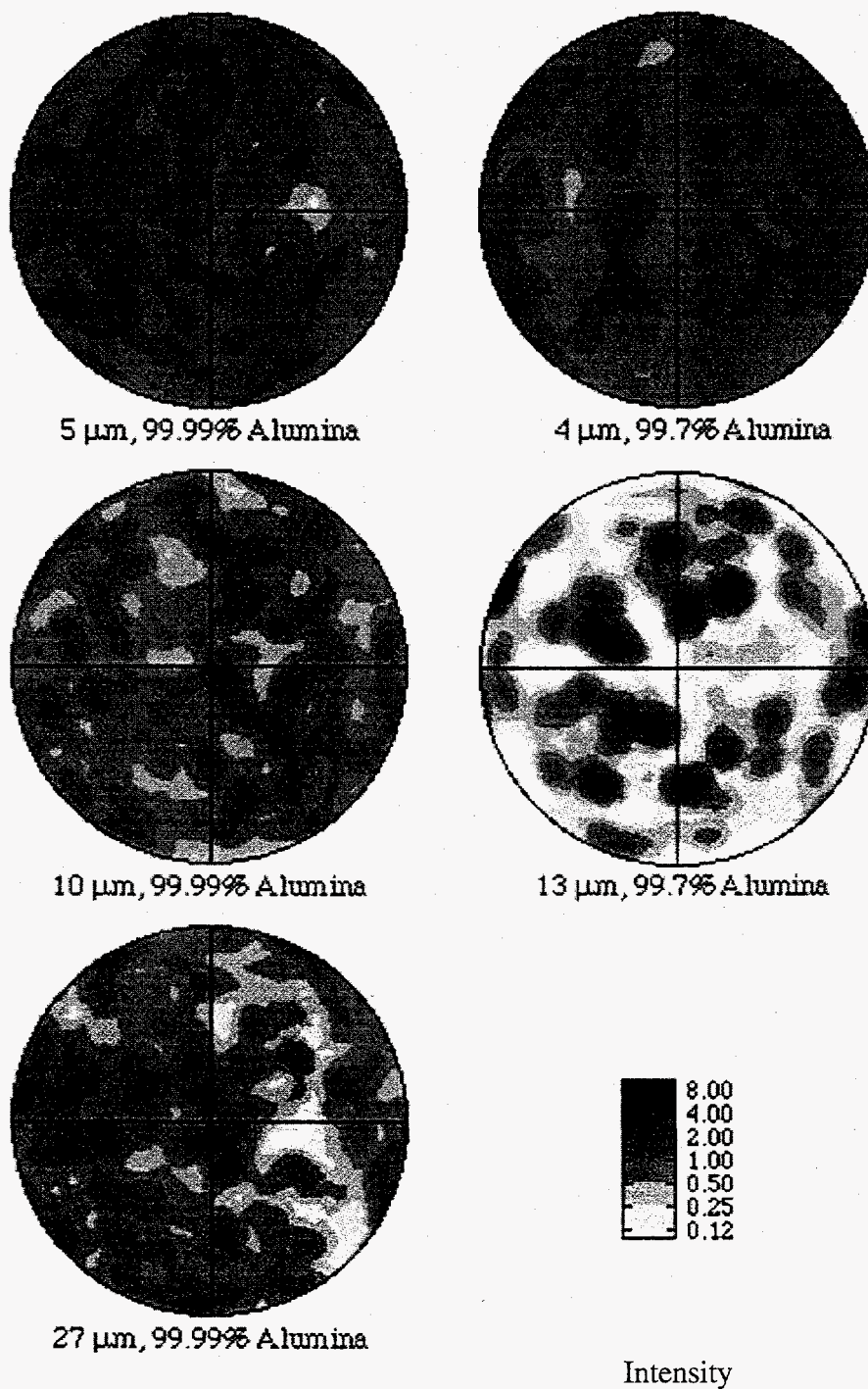
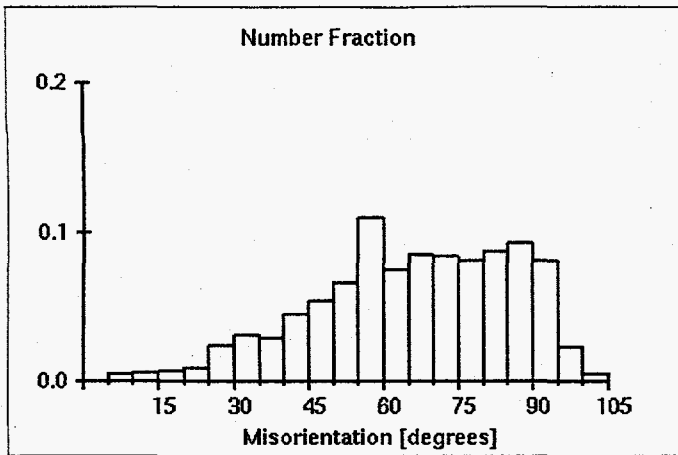
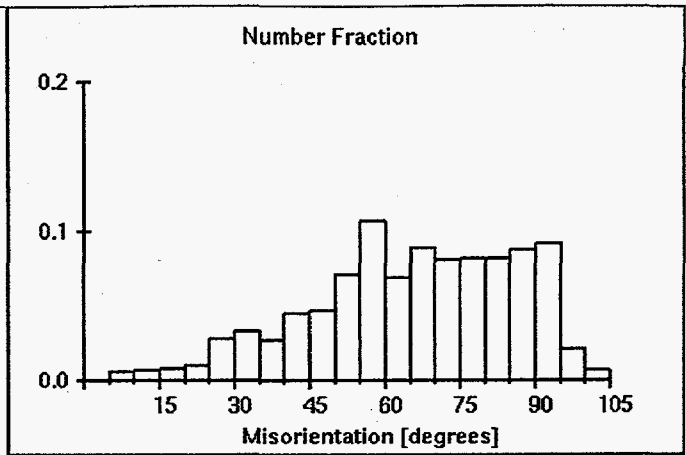


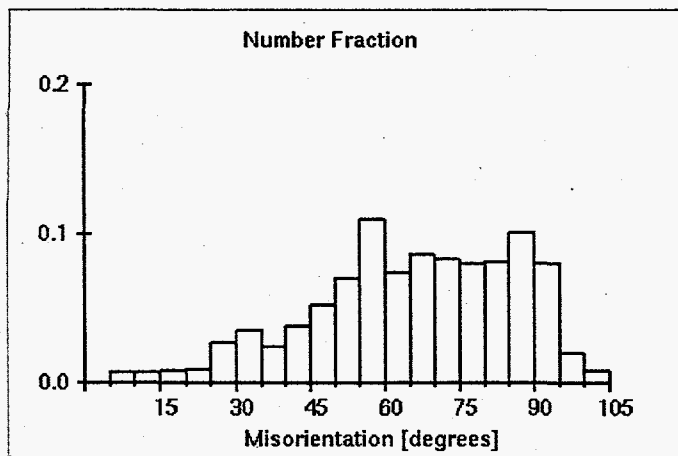
Figure 5. The 002 (using the 3 index notation for trigonal symmetry) intensity pole figures for each of the alumina samples.



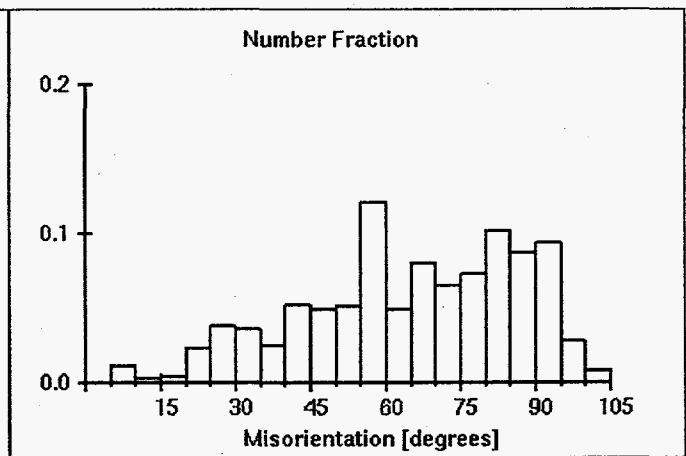
5 μm , 99.99% Alumina



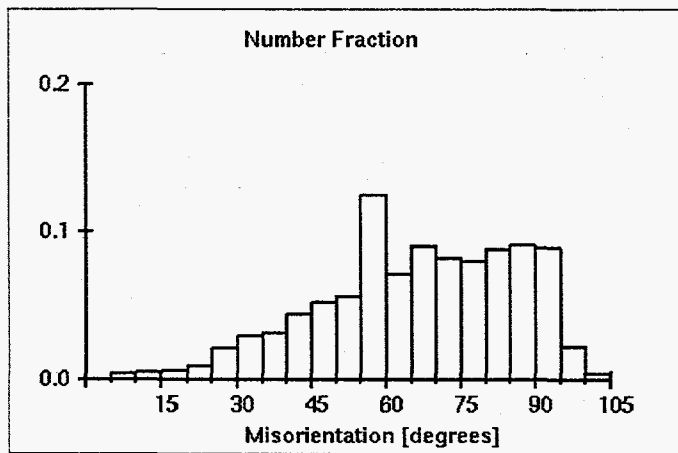
4 μm , 99.7% Alumina



10 μm , 99.99% Alumina



13 μm , 99.7% Alumina



27 μm , 99.99% Alumina

Figure 6. The misorientation distributions as MacKenzie plots for each of the alumina samples.

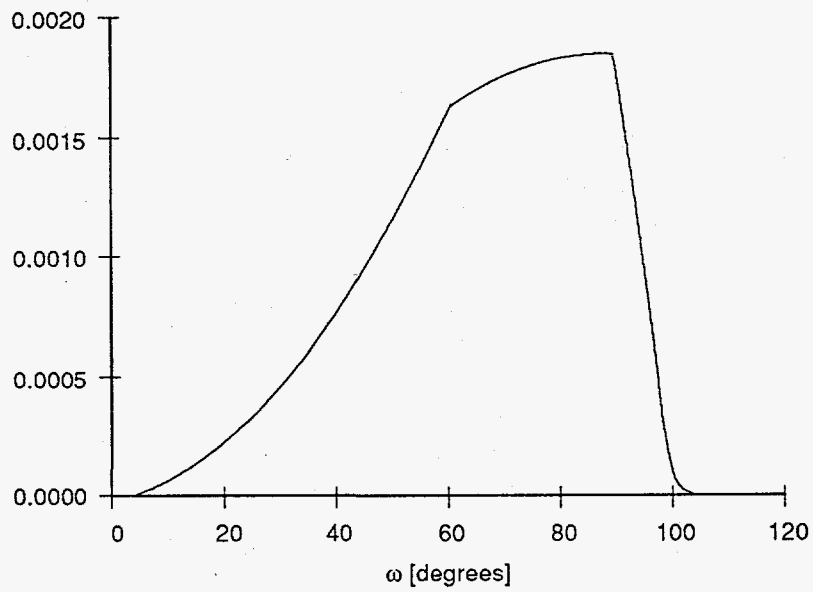


Figure 7. The predicted MacKenzie plot of random misorientations for crystals with 3-fold dihedral symmetry (trigonal).

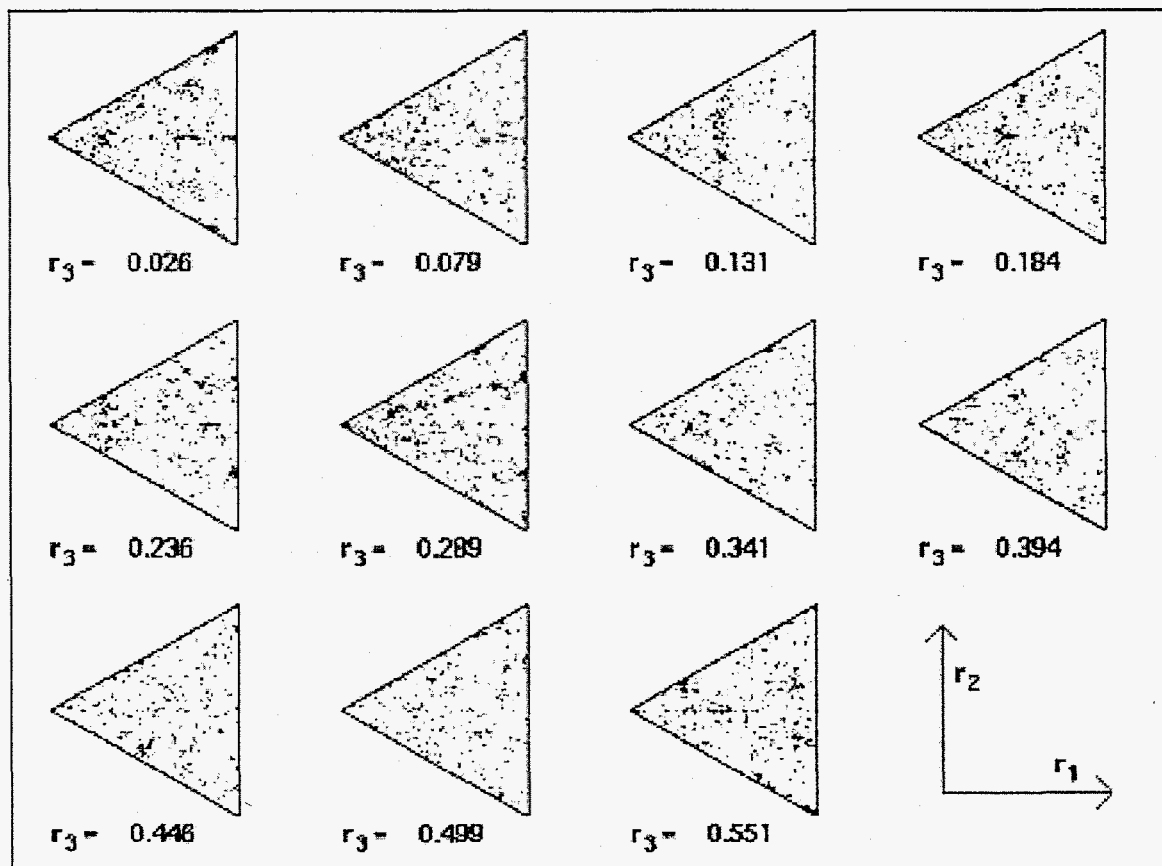


Figure 8.

Misorientation data displayed in Rodrigues space for the 13 μm, 99.7% alumina sample, which appears to exhibit the greatest degree of mesotexture.

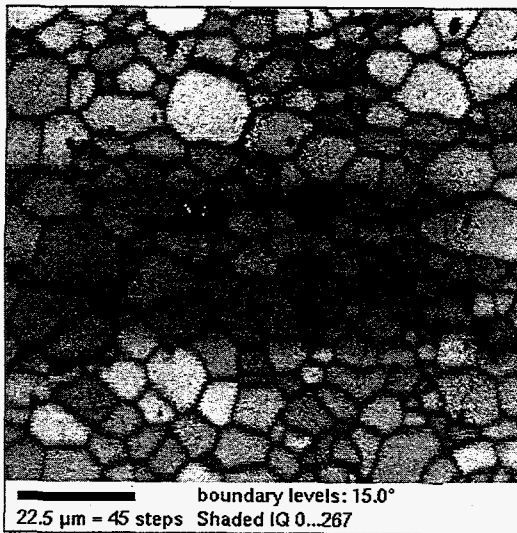


Figure 9. The OIM image of the 10 μm, 99.99% alumina sample and the points across the crack that were used to determine the distribution of misorientations along a crack.

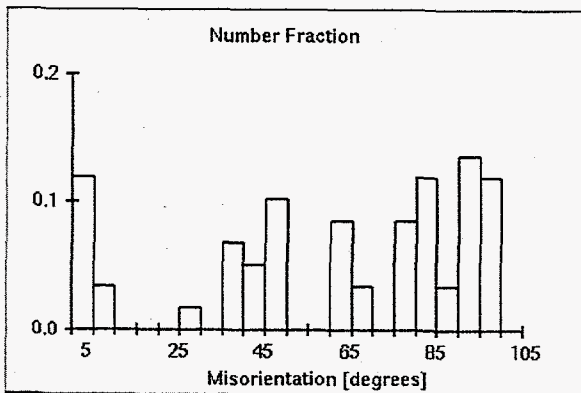


Figure 10. The MacKenzie plot for the misorientations of the crack in Fig. 9. Low angle misorientations represent transgranular fracture. Comparison to the plot in Fig. 6 for the same sample reveals a higher percentage of high angle boundaries.